S. H. Kim
LS - 175

Magnetic Measurement Data of the 0.8-m Prototype Quadrupole Magnets for the APS Storage Ring

1. Summary

From the magnetic measurement data of the two 0.8-m prototype quadrupole magnets (P-SRQ-1 and P-SRQ-2) and the study of the geometries for the pole-end bevels and pole chamfers, the following conclusions have been made.

Mechanical stability of the magnet poles has been achieved by the modification of the weld procedures between two quadrants of the magnets. The stability of the magnet-pole positions was measured optically and was also concluded from the fact that the allowed coefficients, mainly sextupole and octupole terms, were independent of the magnet excitation currents.

The unallowed multipole field coefficients for the second magnet, without any correction of the magnet-pole positions, are smaller than those for the first magnet. The field gradient integrals of the two magnets at 400A differ by less than 5×10^{-4} for r = 2.5 cm. This indicates that an acceptable magnet assembly procedure has been established.

The 2-D calculations and "body" measurements for allowed coefficients after the main field, b_5 and b_9, agree within 1.2×10^{-4} at r = 2.5 cm. This implies that the 2-D design geometry is basically correct and acceptable. As expected for a magnet with long and narrow poles, some saturation effects of pole shims have been observed.

In order to reduce the fabrication cost for the end-plates, the geometries for the pole-end bevels and pole chamfers have been studied. By choosing a bevel angle of 61°, instead of 45°, it is possible to have acceptable allowed coefficients with dimensions of pole-chamfers up to 16.5 mm. This allows the design of the end-plate as one piece without removable pole-tip.

2. Multipole Field Coefficients

The normal and skew multipole field coefficients, b_n and a_n, for a 2-D magnetic field, $B = B_y + iB_x$, are defined

$$BL = B_0 L \sum_{n=0}^{\infty} (b_n + ia_n)(x + iy)^n, \qquad (1)$$

where L is the effective magnetic length, the units of b_n and a_n are in cm^{-n}, $b_1 = 1.0\ cm^{-1}$ and $a_1=0$ for a quadrupole magnet, and $B_0 b_1$ is the main quadrupole field gradient. In order to compare the relative values of the coefficients with respect to the main quadrupole field component, the coefficients are sometimes compared at a particular radius, r_0=2.5 cm,

$$b_n\,(\text{at } r_0) = b_n r_0^n / b_1 r_0, \qquad a_n\,(\text{at } r_0) = a_n r_0^n / b_1 r_0. \qquad (2)$$

Plotted in Fig. 1 are selected multipole coefficients from the measured data for the two prototype magnets. Pole-end bevels with a geometry of 12.8 mm x 12.8 mm (45°-cut) are used for both ends of the magnets. Measurements #2 and #4 for SRQ-1 were conducted at Fermilab, and those of #5-1 for SRQ-1 and #1-1 for SRQ-2 at ANL-362HB. A rotating coil method was used for all the measurements.

Detailed descriptions of the legends in Fig. 1 are listed in Table 1. The descriptions in Table 1 are understood from Fig. 2 which shows the end-view of the current-lead side (a), pole-face geometry (b), and an end-view of the top-half section (c) of the magnet. The two prototypes have the same pole face geometry. In the assembly of the upper and lower halves of the magnet, Al-blocks are inserted between the two halves in the right-hand side of the magnet in Fig. 2 (a). The left side of the magnet between the two halves is supported by Al-rods. Prior to the final assembly, each half of the magnet was assembled by welding the stacked laminations of the two quadrants of the magnet.

Table 1. Details of the legends in Fig.1. Al-blocks and Al-rods are inserted in the right and left sides of the magnet shown in Fig.2 (a). Positive and negative numbers for the Al-blocks or Al-rods in the table represent a increase or decrease of the gap between the two halves of the magnet.

Measurement #		Description
P-SRQ-1	#2-1	Reference measurement
	#2-3	Al-block: -0.25mm, Al-rod: -0.25mm
	#2-6	Al-block: -0.25mm, Al-rod: 0.0, upper two poles were moved 0.13mm toward Al-block side
	#2-8	Al-block: -0.25mm, Al-rod: +0.13mm, upper two poles were moved 0.064mm toward Al-block side
	#4-3	Reference measurement after additional welding of the laminations
	#4-4	Al-block: -0.13mm, Al-rod: -0.13mm
	#4-21	Al-block: -0.13mm, Al-rod: 0.0
	#4-22	Al-block: 0.0, Al-rod: -0.13mm
	#4-23	Al-block: +0.13mm, Al-rod: 0.0
	#4-24	Al-block: +0.25mm, Al-rod: 0.0
	#5-1	Repeated measurement of #4-24
P-SRQ-2	#1-1	Reference measurement

Variations of the coefficients, $b_2 \sim b_4$ (sextupole ~ decapole) in Fig. 1 (a) and (b) for measurement #2 SRQ-1 at different currents, are attributed to the movements of the magnet poles. Optical measurements of the pole movements were approximately 0.11mm ~ 0.18mm.

After additional welding at "B" between the stacked laminations of the two quadrants of the half-magnets in Fig. 1 (c), pole movements in the Al-rods side in the vertical direction were less than 0.02mm. No appreciable pole movements were observed in the horizontal direction. The data of measurements #4 and #5 for SRQ-1, which were measured after the additional welding, show that $b_2 \sim b_4$ are stabilized compared to those for measurement #2, the skew sextupole coefficient a_2 in particular.

The data of measurement #1-1 for SRQ-2 also shows that $b_2 \sim b_4$ do not have any significant variation in current. Pole movements in the Al-rods side of SRQ-2 were less than 0.05mm.

Coefficients b_5 and b_9 (duodecapole and 20-pole) are the first two allowed coefficients after the main field for a symmetrical quadrupole magnet. As expected for long and narrow poles, both coefficients in Fig. 1 (c) show some degree of saturation effects at higher currents.

Shown in Figs. 3 and 4 are the relative magnitudes of the coefficients at a radius of 2.5cm, defined by Eq. (2), for SRQ-1 and SRQ-2, respectively. By comparing the two figures, it is seen that the field quality of SRQ-2, even without any correction of the pole positions, is improved to some degree, compared to that of SRQ-1. The two largest unallowed coefficients for SRQ-2 are normal sextupole and octupole terms, $b_2 = 2.5 \times 10^{-4}$ and $b_3 = 3.5 \times 10^{-4}$ at r = 2.5 cm.

3. Magnetic Excitation

Plotted in Fig. 5 are the field gradient integral vs. excitation current and the excitation curve normalized to the current. Above 300A, the gradient integrals of the two magnets differ by less than 5×10^{-3}. One standard deviation of the gradient integral measurements at 400A is less than 5×10^{-4}. It is seen from the figure that above 300A, the excitations of the magnets start to saturate considerably.

Figure 6 shows the data for 2-D body field measurements for SRQ-1. The middle of the iron yoke in the longitudinal direction is located at approximately z = 0. The length of the yoke is 0.765m. A data point in the figure represents the field gradient integral from the data point at z to the left end of the magnet in the field free region. The data were taken by moving the probe coil along the z-direction with a position accuracy $\Delta z = \pm$ 0.5mm. The slope of a linear extrapolation of the data represents an average field gradient for a given length of the magnet.

In Table 2, the field gradients normalized to the excitation currents of the magnets, B'/I, are listed. The field gradients were calculated from the data in Fig. 6 as average values for the specified segments in the z-axis. The normalized field gradient for $\mu = \infty$ is calculated

$$B_0'/I = \frac{2\mu_0}{a^2} N/\text{pole} \qquad (3)$$

$$= 5.18363 \times 10^{-2}\ (T/m\cdot A),$$

where $N = 33$ turns and $a = 40 \times 10^{-3}$m for the radius of the aperture of the two magnets. The relative saturation of the field gradient (or field), B'/B_0', is also listed in the table. It is seen that the saturation for $z > 0.27$m at 450A is significant. Two-dimensional calculation of the efficiency at 450A is 88.5% [1], compared to the measured data of 87.16% shown in the table for $z < 0.215$m.

Table 2. Field gradients at different segments of the magnet normalized to the excitation currents, which were calculated from the data in Fig. 6. B'/B_0', is the ratio of the field gradient from Fig. 6 and that for $\mu = \infty$.

	250.79A		450.75A	
z (m)	$B'/I(T/m\cdot A)$ (10^{-2})	B'/B_0'	$B'/I(T/m\cdot A)$ (10^{-2})	B'/B_0'
0 ~ 0.215	5.1220	0.9881	4.518	0.8176
0.215 ~ 0.27	5.1005	0.9840	4.4851	0.8651
0.27 ~ 0.325	4.993	0.9632	4.2083	0.8118

If one uses the normalized field gradient for $z = 0 \sim 0.215$m at 250.79A as the reference, $B'/I = 5.122 \times 10^{-2}$ T/m·A, the effective magnetic length calculated from the field gradient integral at the same current is

$$L = 0.79364 \text{ m}$$
$$= 0.765 \text{ m (length of the iron yoke)} + \alpha\, a, \qquad (4)$$

where $\alpha = 0.716$. Note that α is typically between 1.0 (for unsaturated magnet) and 0.6 (for saturated magnet).

From the requirements for the storage ring quadrupole magnets and from the magnetic measurement data for SRQ-1 shown in Fig. 1, parameters for the magnets, Q1, Q2, Q3, Q4 and Q5, for the operation at 7-Gev are listed in Table 3. It is seen that the excitation efficiencies for Q4 and Q5 are relatively lower compared to those for other magnets in the table.

Table 3. Parameters of the storage ring quadrupole magnets for 7-Gev operation.

	Q1	Q2	Q3	Q4	Q5
L (m)	0.50	0.80	0.50	0.50	0.60
B′ (T/m)	-10.8427	15.7919	-10.585	-18.902	18.2479
B′L (T)	-5.421	12.634	-5.293	-9.451	10.949
I (A)	215	320	210	415	390
Efficiency(%)	99	97.5	99	89	92

4. 2-D Calculations and "Body" Measurements

Both of the magnets have pole-end bevels with a geometry of 12.8 mm x 12.8 mm - cut ($\Delta r = \Delta z = 12.8$ mm in Fig. 7 (a)). For SRQ-1, this bevel geometry increases b_5 by 1.4×10^{-5} cm^{-5} (5.5×10^{-4} at r = 2.5 cm) and reduces b_9 by 1.0×10^{-8} cm^{-9} (-0.15×10^{-4} at 2.5 cm) compared to the measurment data without the cut. The measured data for b_5 and b_9 from the body and end contributions at four selected currents for SRQ-1 are listed in Table 4.

Figure 8 shows the body values of the two allowed coefficients b_5 and b_9 for the two magnets. The first magnet was measured at Fermilab (Body-F Q-1) and repeated using a new probe fabricated in-house (Body ANL1 Q-1). The second magnet was measured using the new probe (Body ANL1-1 Q-2). The two coefficients for integral measurements, shown in Fig. 1 (c) #5-1 Q-1 and #1-1 Q-2, are also plotted in Fig. 8 to compare with the body values.

Table 4. Body and end contributions for b_5 and b_9 from SRQ-1 data (numbers in parentheses are relative values of the coefficients with respect to the main quadrupole field at r = 2.5 cm in 10^{-4} unit). The pole-end bevels have a geometry of 12.8 mm x 12.8 mm-cut.

	103A	250A	400A	450A
b_5 (10^{-6})				
Body	-1.96 (-0.77)	-2.15 (-0.84)	-3.79 (-1.48)	-4.54 (-1.77)
Body+Ends	0.52 (0.20)	0.28 (0.11)	-1.98 (-0.77)	-3.02 (-1.18)
Ends	2.48 (0.97)	2.43 (0.95)	1.81 (0.71)	1.52 (0.59)
b_9 (10^{-8})				
Body	-2.91 (-0.45)	-2.93 (-0.45)	-3.17 (-0.49)	-3.35 (-0.51)
Body+Ends	-3.38 (-0.52)	-3.43 (-0.52)	-3.77 (-0.58)	-3.95 (-0.60)
Ends	-0.47 (-0.07)	-0.50 (-0.07)	-0.60 (-0.09)	-0.60 (-0.09)

Considering the contribution of the ends and body+ends to b_5, the geometry chosen for the pole-end bevels is quite adequate. The dependence of b_9 on the end geometry is relatively small. Figure 8 and Table 5 show that the 2-D calculations and body measurments for the two allowed coefficients agree within 1.2×10^{-4} at r = 2.5 cm. This implies that the design of the 2-D pole face is basically correct and adequate.

Table 5. 2-D calculations for allowed coefficients b_5 and b_9 (numbers in parentheses are relative values at r = 2.5 cm in 10^{-4} unit) [1].

	at "low" excitation	at 410 A
b_5 (10^{-6})	0.34 (0.132)	-0.86 (-0.335)
b_9 (10^{-8})	4.73 (0.719)	4.51 (0.686)

5. Pole-End Bevels and Pole Chamfers

In order to reduce the length of the magnet coils, the end-plates of the prototypes have 19.9 mm-45°-cut pole chamfers as shown in Fig. 2 (c). The removable pole-tip shown in the figure has pole-end bevel of 12.8 mm x 12.8 mm-cut, as mentioned in the previous sections. But it does not have pole chamfers. Therefore, the pole-tips should be attached to the end-plates only after the installation of the magnet coils.

The fabrication cost for the end-plates can be reduced if the pole-tips are not a removable-type. This requires extension of the pole chamfers to the pole-tips not increase in the length of the magnet coils. The end-bevels for a geometry of 45°-cut have been studied in detail by Hassenzahl [2]. Our purpose is to determine the end-bevel geometry with pole chamfers of at least 12.8 mm in order not to change the coil length.

Figure 9 compares the dependence of b_5 on bevel geometries and body (2-D) values for SRQ-1. The changes of the coefficient for 12.8 m m x 12.8 mm-bevels (45°) were discussed already in section 4. Since 9.6 mm x 17.4 mm-bevels (61°) are more efficient than 45°-bevels, as shown in Fig. 9, 61°-bevel geometry has been chosen for the study of pole chamfers (see Fig. 7 (a) for the bevel angle).

Plotted in Fig. 10 is the dependence of b_5 on the dimensions of the 61°-bevels and on the largest bevel (9.6 mm x 17.4 mm) with three different cuts of pole chamfers. Figure 7 (b) shows a drawing of the largest bevel with 12.8-mm pole chamfers for the removable pole-tip. If one chooses a pole chamfer of 12.8 mm ~ 16.5 mm for the largest bevel, it is seen from Fig. 10 that the end effect of b_5 can be removed. This geometry is equivalent to end bevels of approximately 4.8 mm x 8.8 mm-cut without any pole chamfers.

In Table 6, b_5 and b_9 are listed for selected pole-end geometries. Some of the values for b_5 are shown already in Figs. 9 and 10. The table shows that the variations of b_9 for the different end-geometries are relatively insensitive compared to those of b_5; its variation is less than 0.4×10^{-4} at r = 2.5 cm.

Table 6. Pole-end bevels on the removable pole-tips and corresponding b_5 (10^{-6}) and b_9 (10^{-8}) coefficients from integral measurements for SRQ-1 at two excitation currents (numbers in parentheses are values ar r = 2.5 cm in 10^{-4} unit).

	250.7 A		450.6 A	
End bevels with chamfers (mm)	b_5	b_9	b_5	b_9
(a) 12.8 x 12.8 (45°)	0.48	-3.50	-2.92	-3.87
	(0.19)	(-0.54)	(-1.14)	(-0.59)
(b) 9.6 x 17.4 (61°)	6.82	-4.12	2.92	-4.46
	(2.66)	(-0.63)	(1.14)	(-0.69)
(c) 9.6 x 17.4	0.23	-4.68	-2.80	-5.11
with 12.8 chamfers	(0.09)	(-0.72)	(-1.09)	(-0.78)
(d) 9.6 x 17.4	-1.78	-5.35	-5.09	-5.44
with 16.5 chamfers	(-0.70)	(-0.82)	(-1.99)	(-0.84)
(e) 9.6 x 17.4	-6.08	-5.68	-9.82	-5.77
with 19.1 chamfers	(-2.37)	(-0.87)	(-3.83)	(-0.89)

6. Reference

[1] Calculated by L. R. Turner.

[2] W. V. Hassenzahl, " An Algorithm for Eliminating the Duodecapole Component in Quadrupole Magnets," Proceedings in the 4th International Conference on Magnet Technology, Brookhaven, 1972, pp. 469-474.

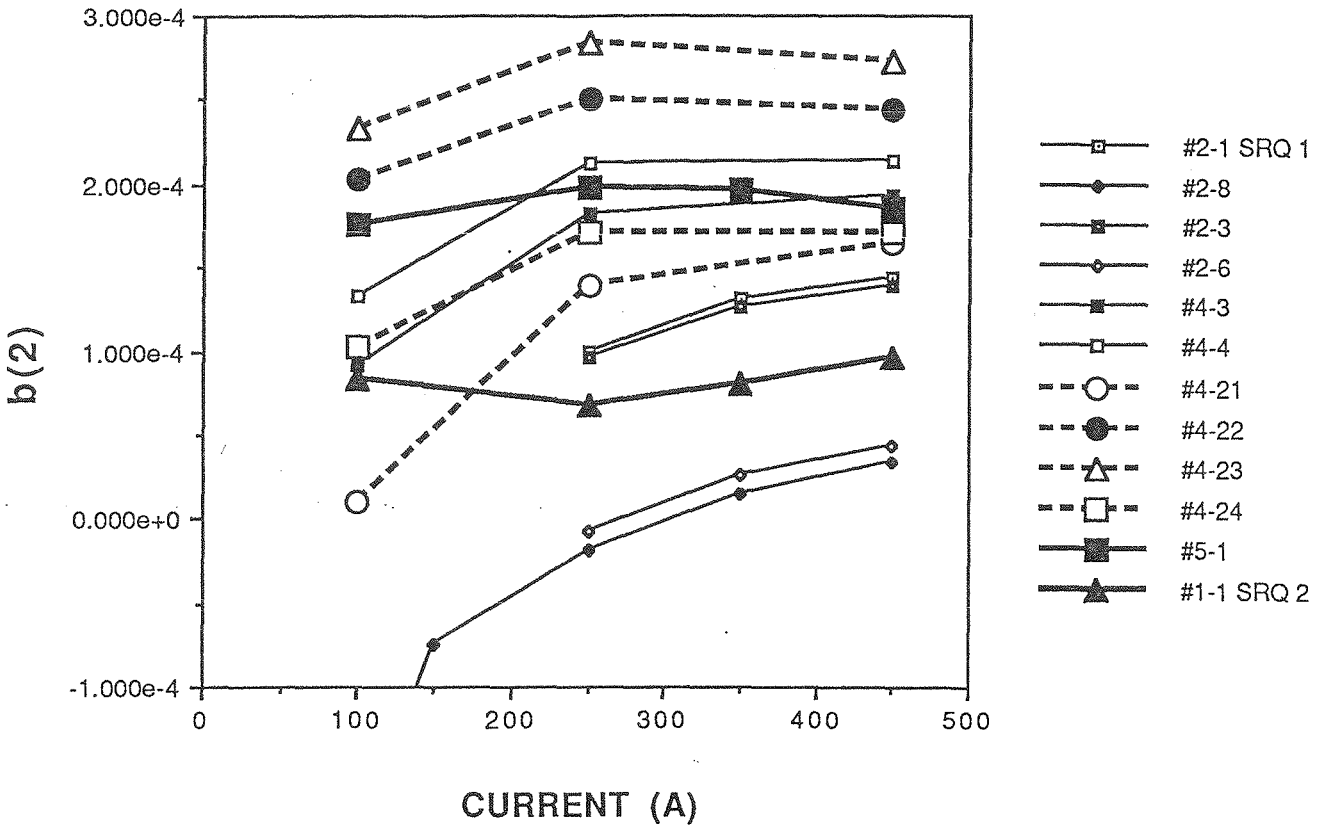

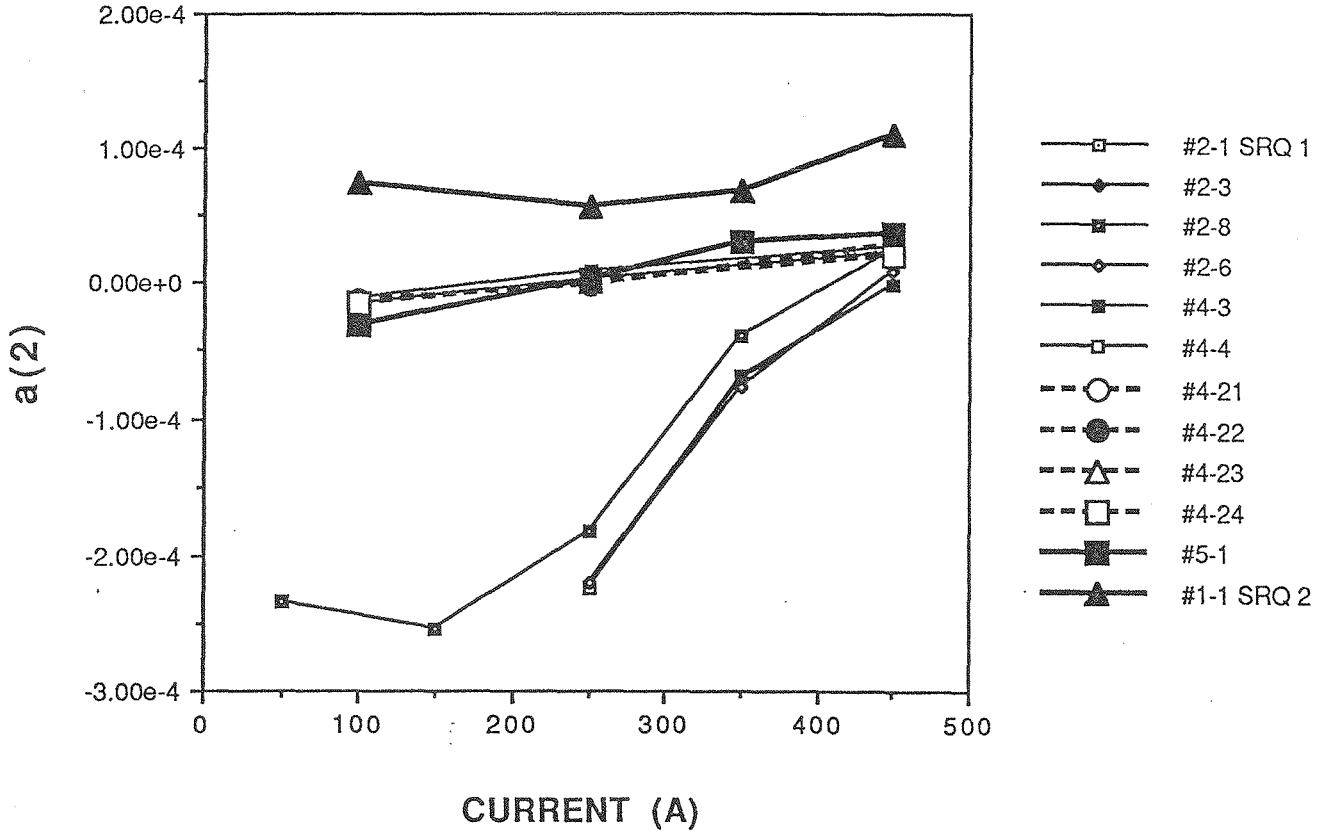

Fig. 1. Multipole field coefficients. Details of the legends are listed in Table 1.
(a). Normal and skew sextupole coefficients.

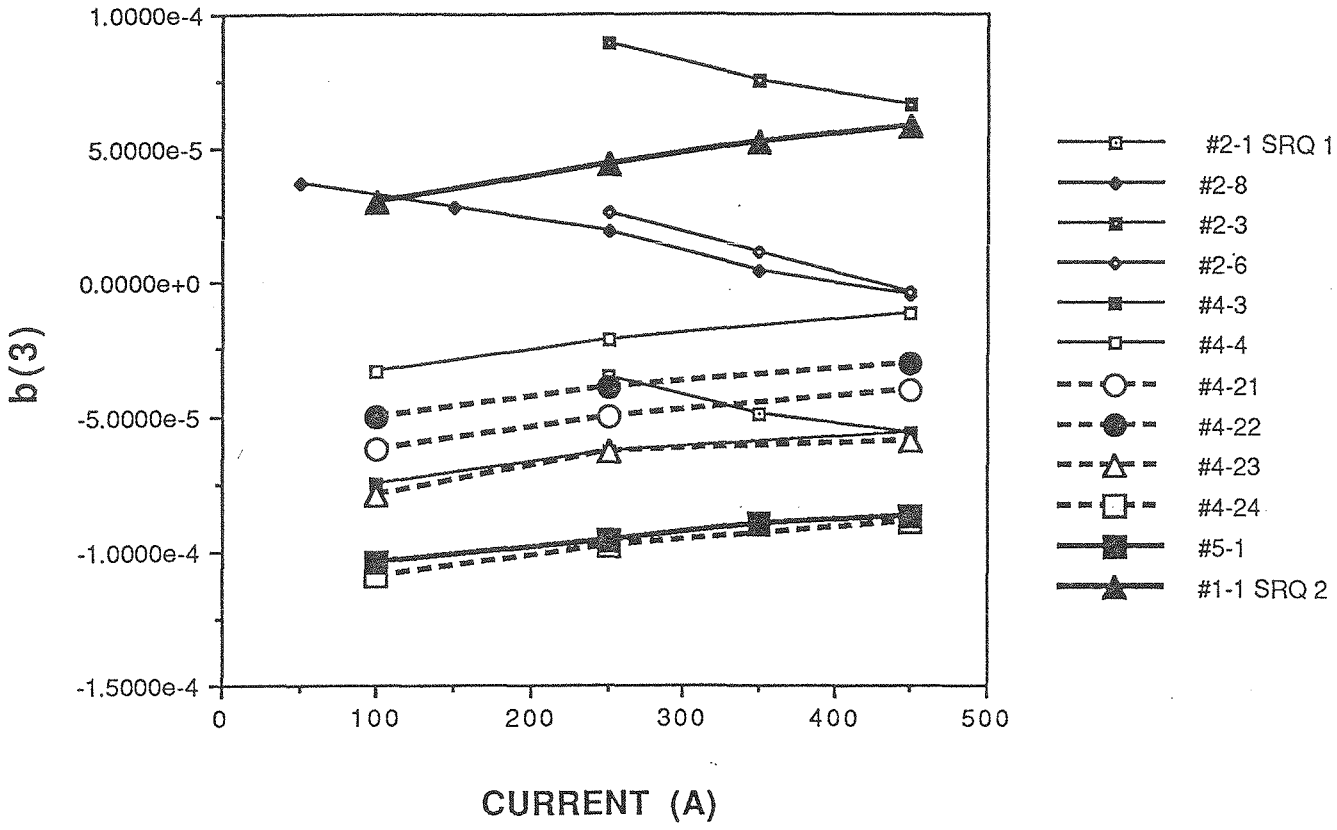

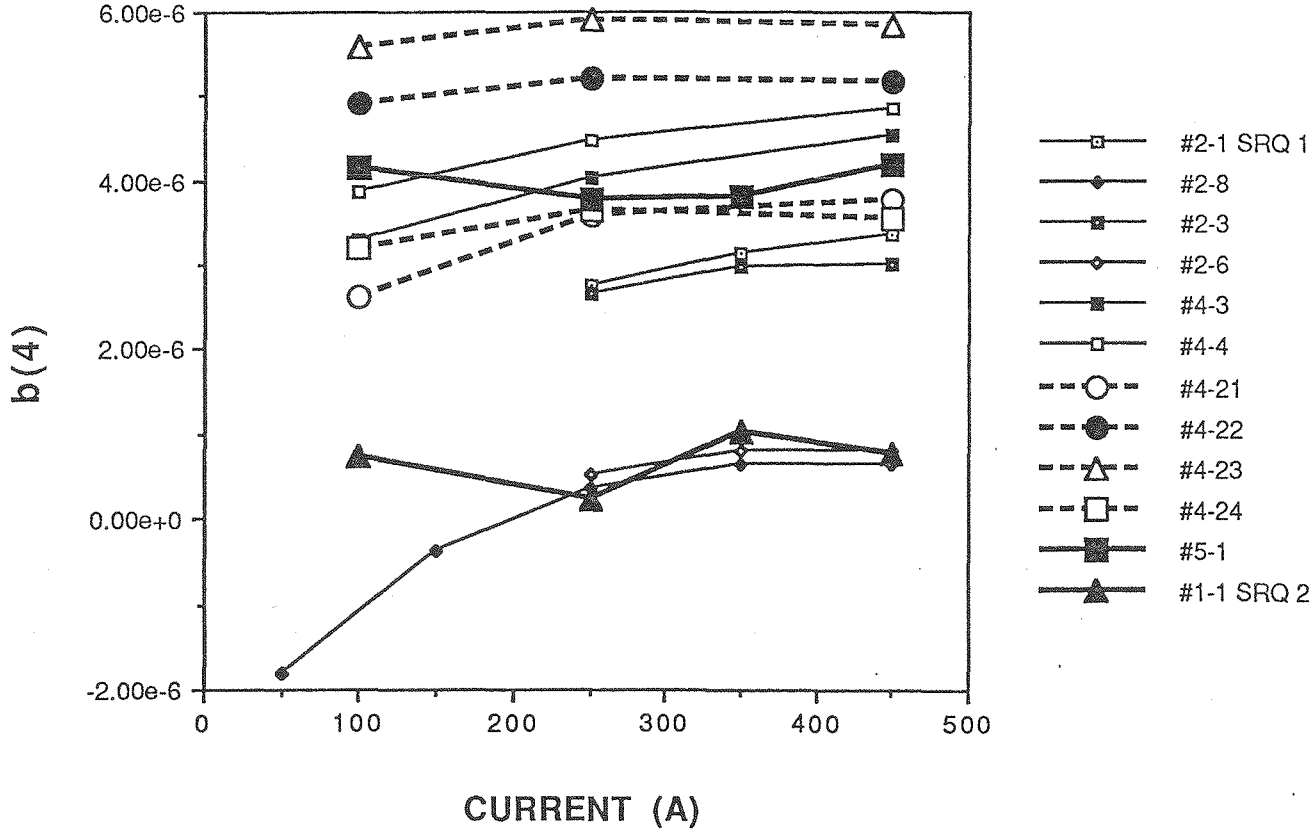

Fig. 1 (b). Normal octupole and decapole coefficients.

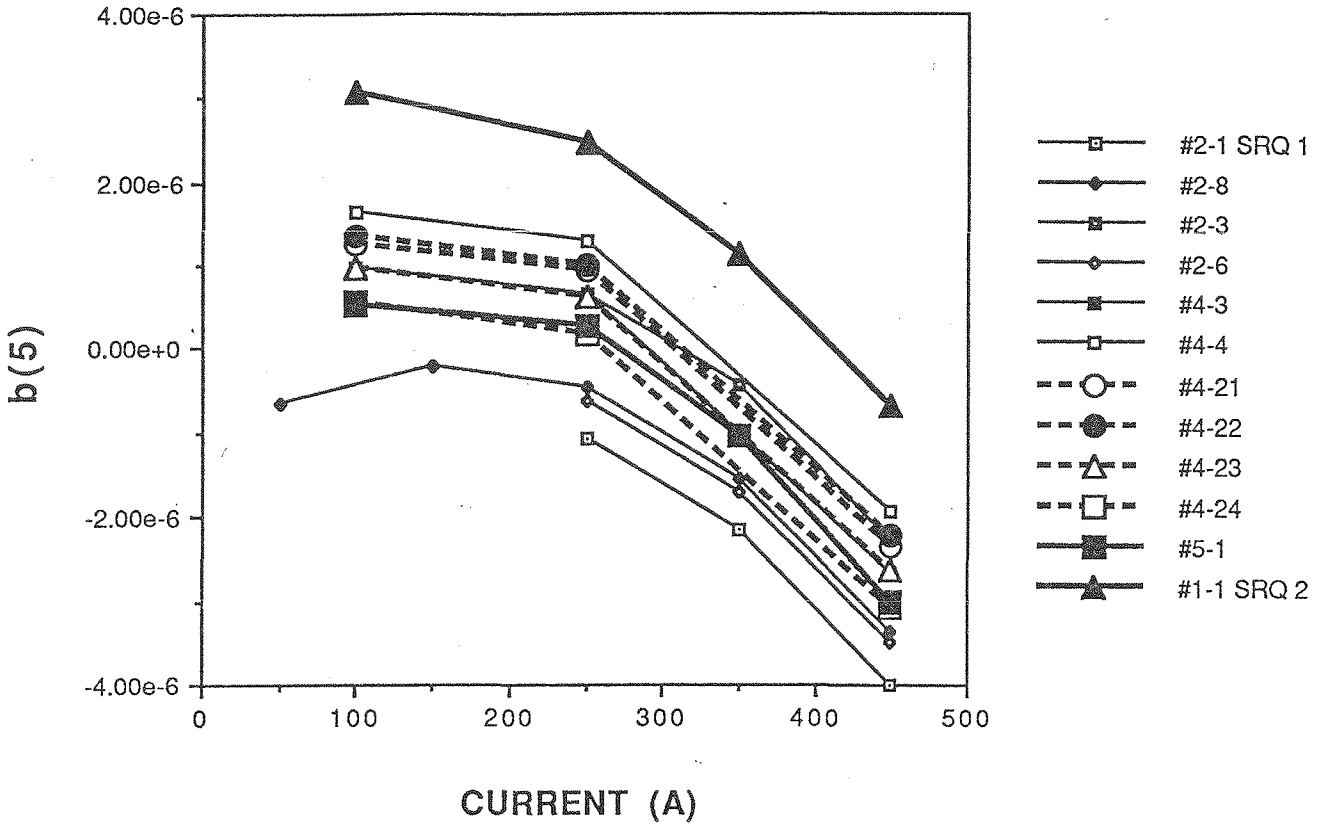

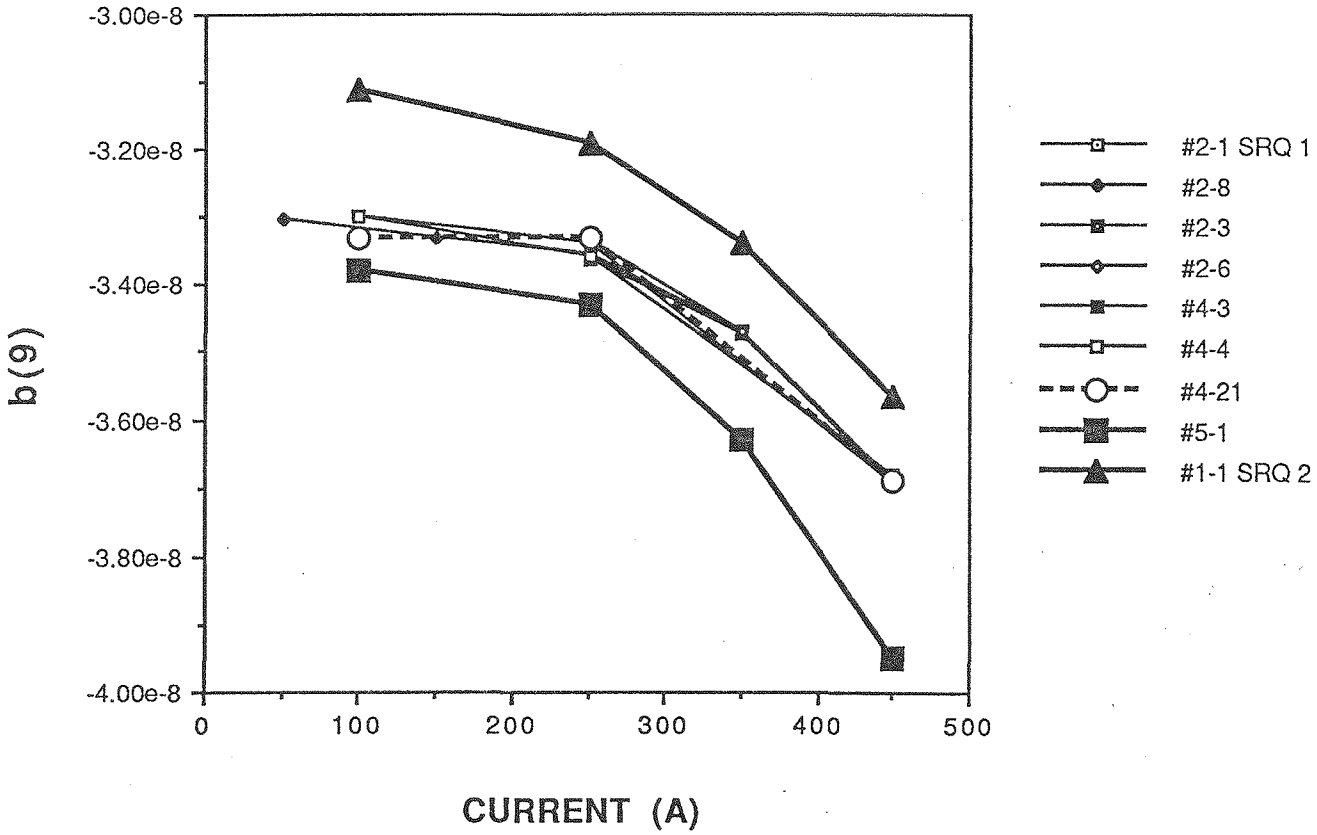

Fig. 1 (c). Normal duodecapole and 20-pole coefficients.

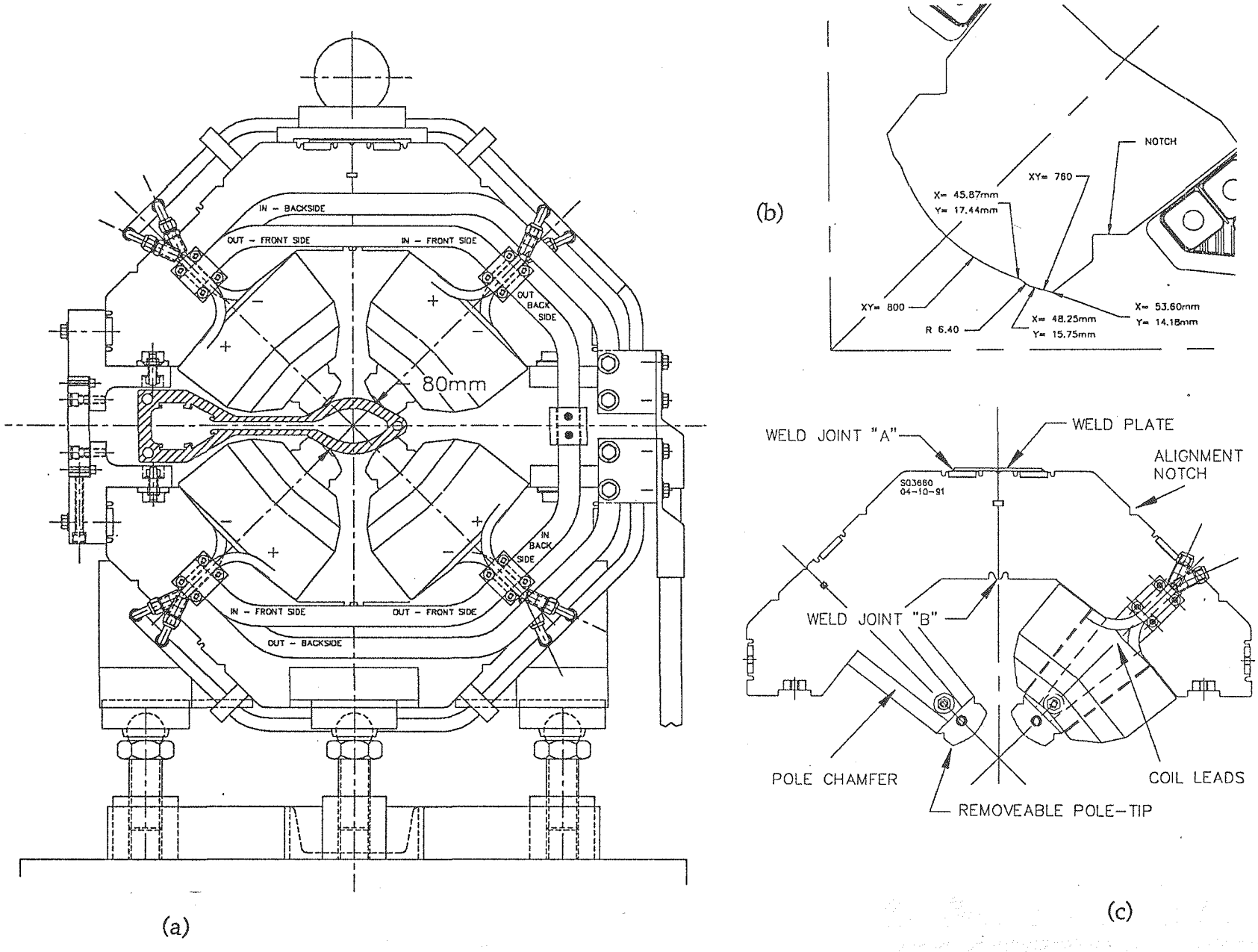

Fig. 2. End-view (a), pole-face geometry (b), and end-view of the top-half section (c) of the prototype quadrupole magnet for the storage ring.

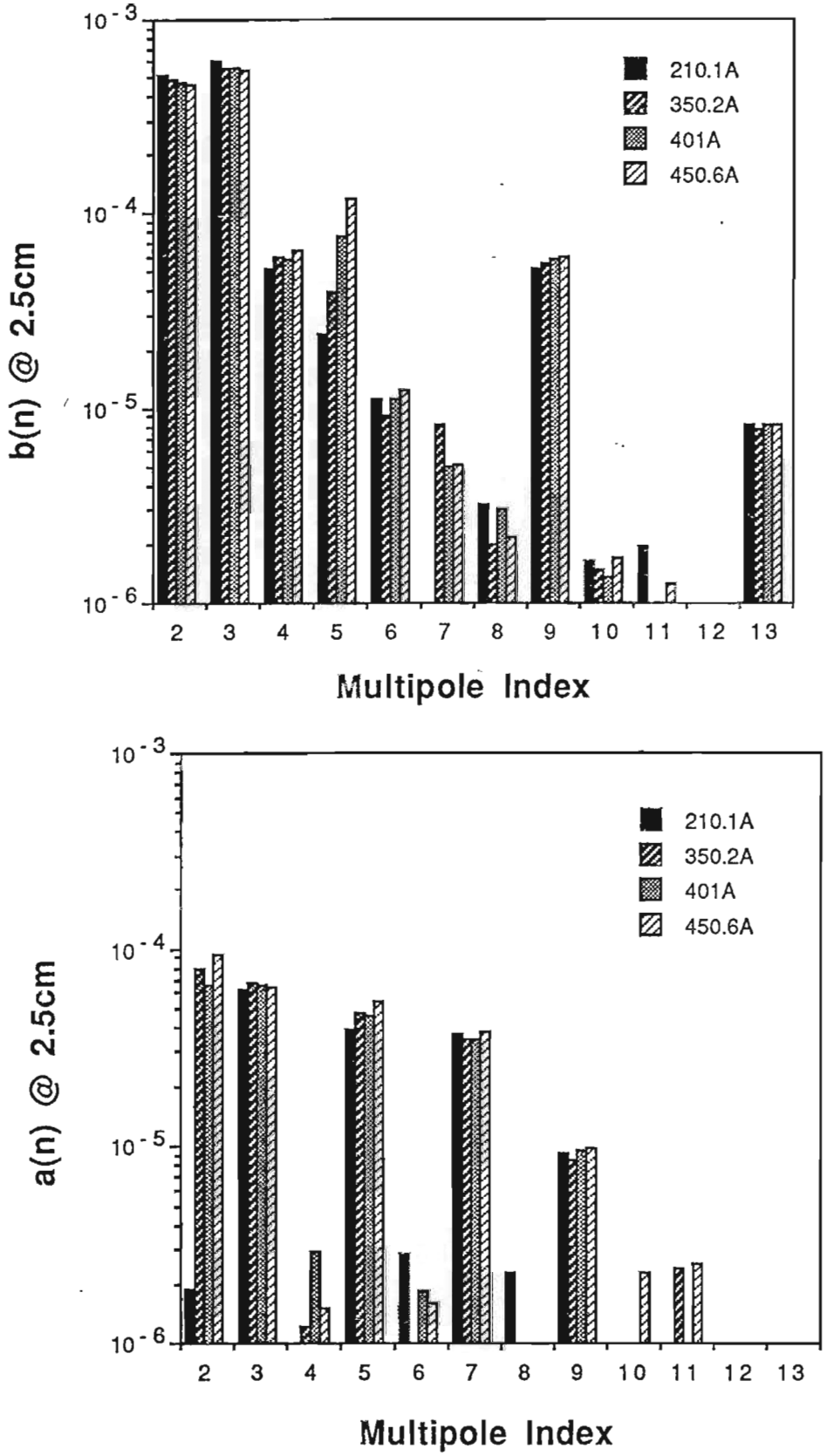

Fig. 3. Magnitude of the relative multipole coefficients with respect to the quadrupole field component for P-SRQ-1 at r = 2.5 cm. The following coefficients have negative values: b_3, b_5 except at 210.1A, b_8, b_9, b_{11}, b_{13}, a_2 at 210.1A, a_3, a_4, a_6, and a_8.

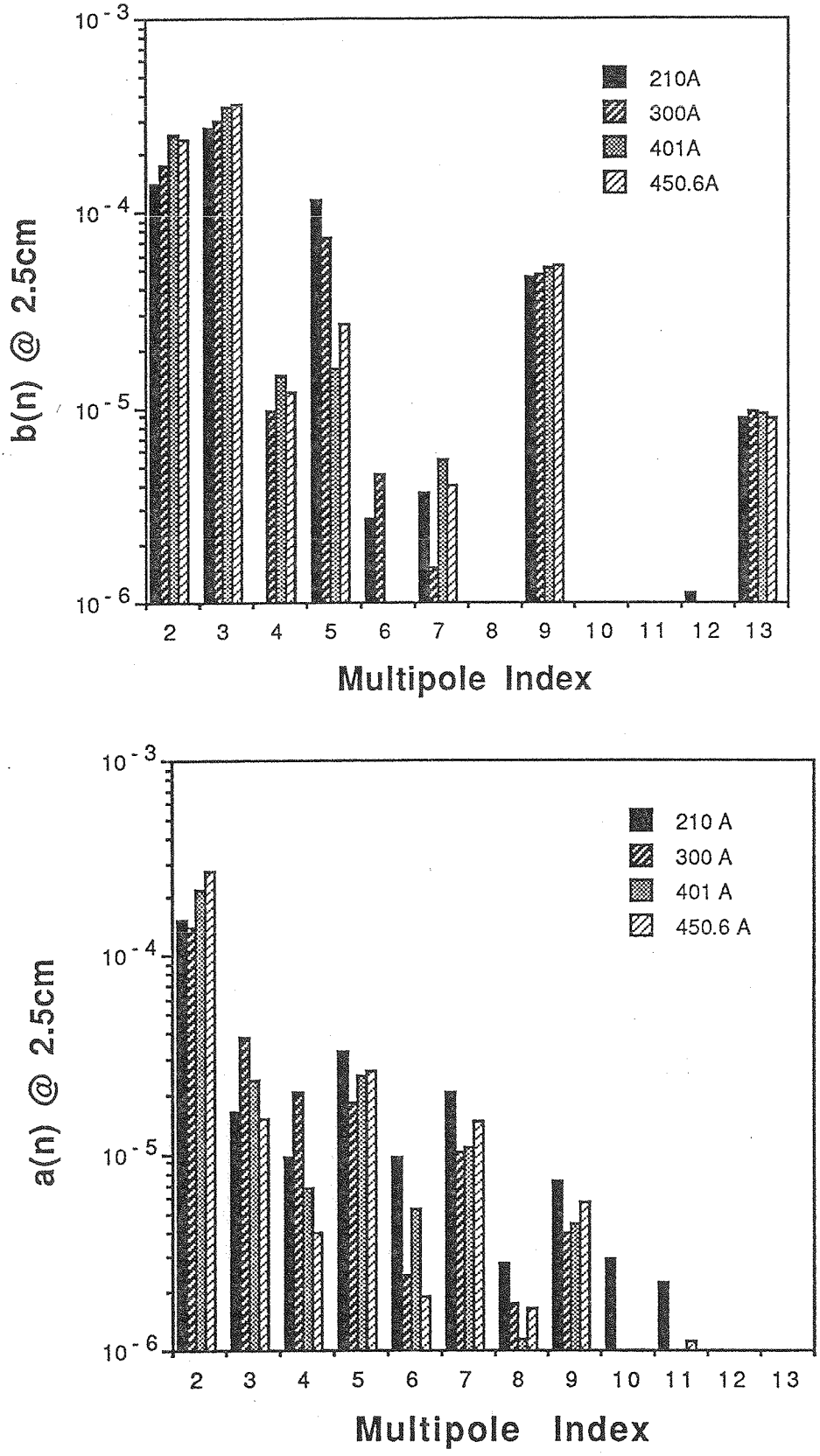

Fig. 4. Magnitude of the relative multipole coefficients with respect to the quadrupole field component for P-SRQ-2 at r = 2.5 cm. The following coefficients have negative values: b_5 at 450.6A, b_6, b_9, b_{13}, a_3, a_4 except at 210A, a_6, a_8 at 410A and 450.6A, a_9 450.6A, and a_{10}.

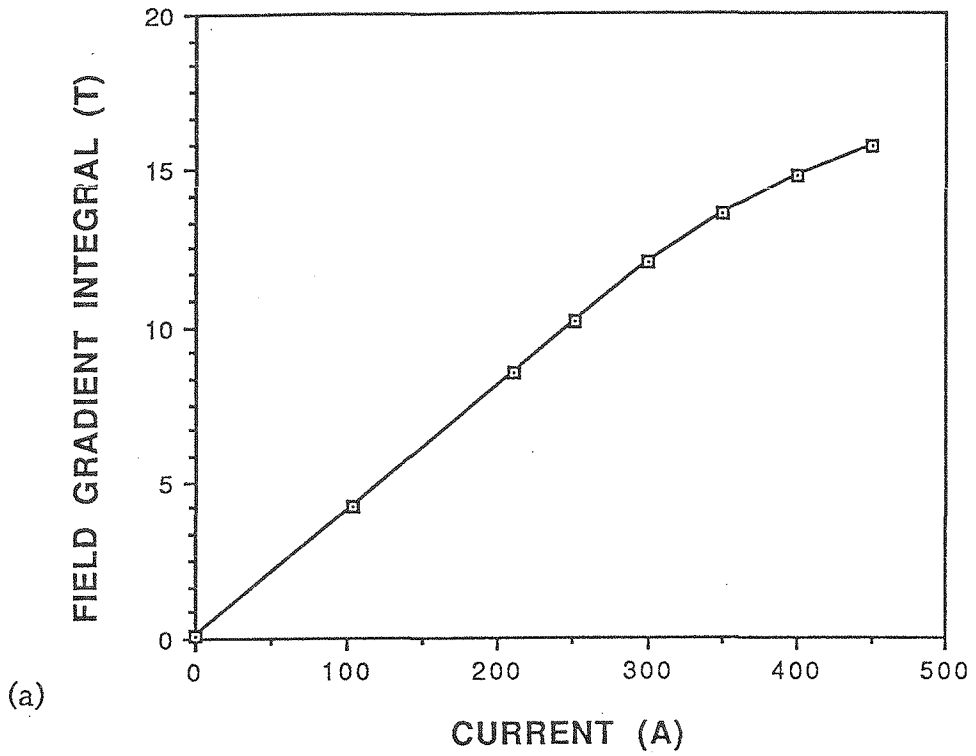

(a)

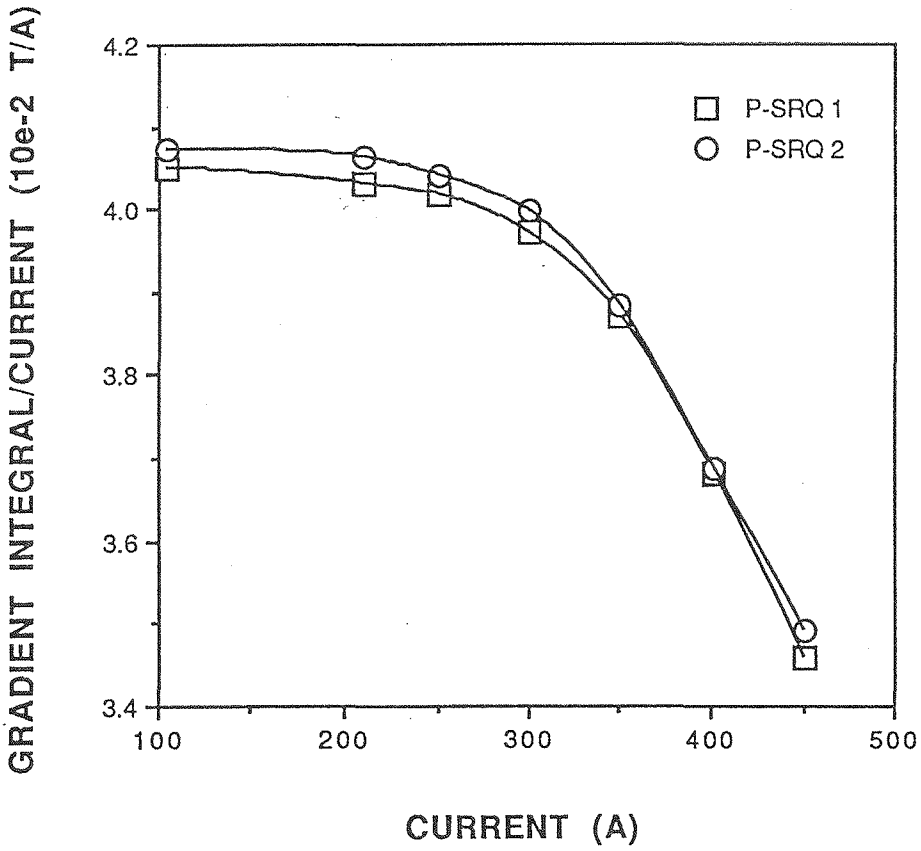

(b)

Fig. 5. Magnet excitation curve (a) and the normalized curves to the excitation currents (b) for the two prototype magnets.

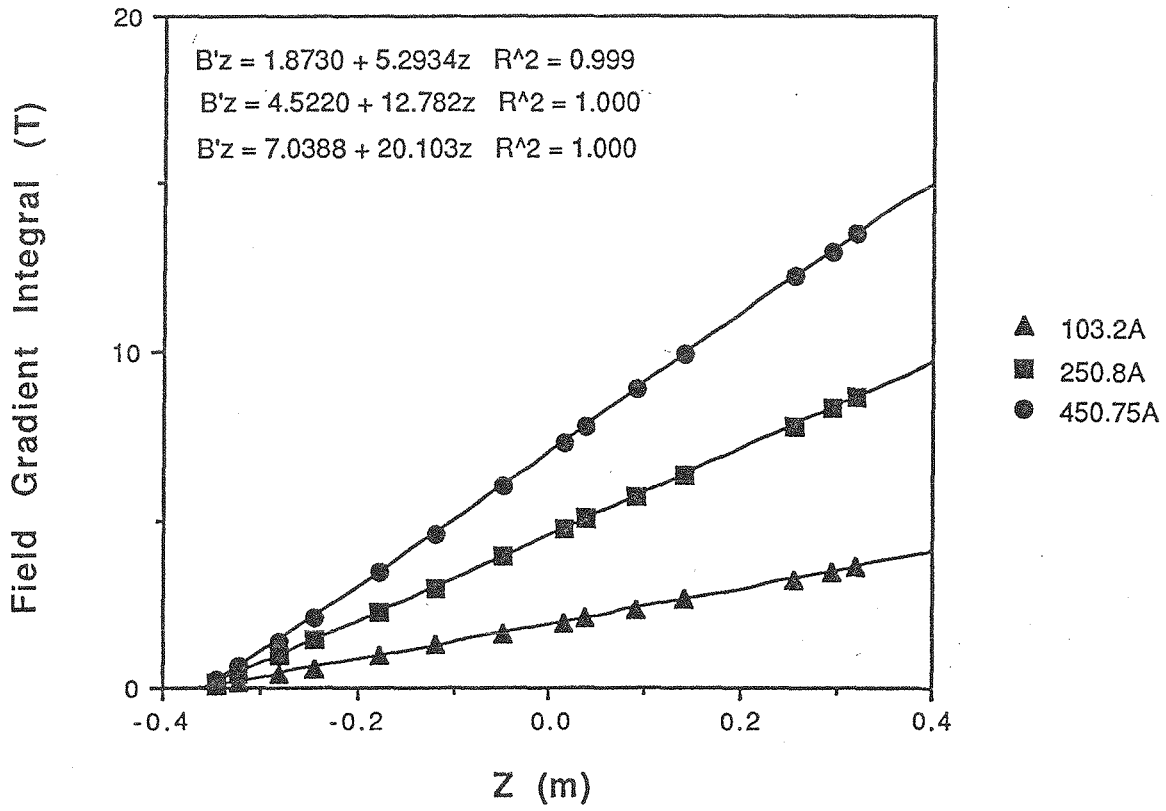

Fig. 6. Data for the body-field gradient measurements for P-SRQ-1. Middle of the iron yoke is located at z = 0. A data point in the figure represents the field gradient integral from the data point at z to the left end of the magnet in the field free region. Field gradient is calculated from the slope of the data points.

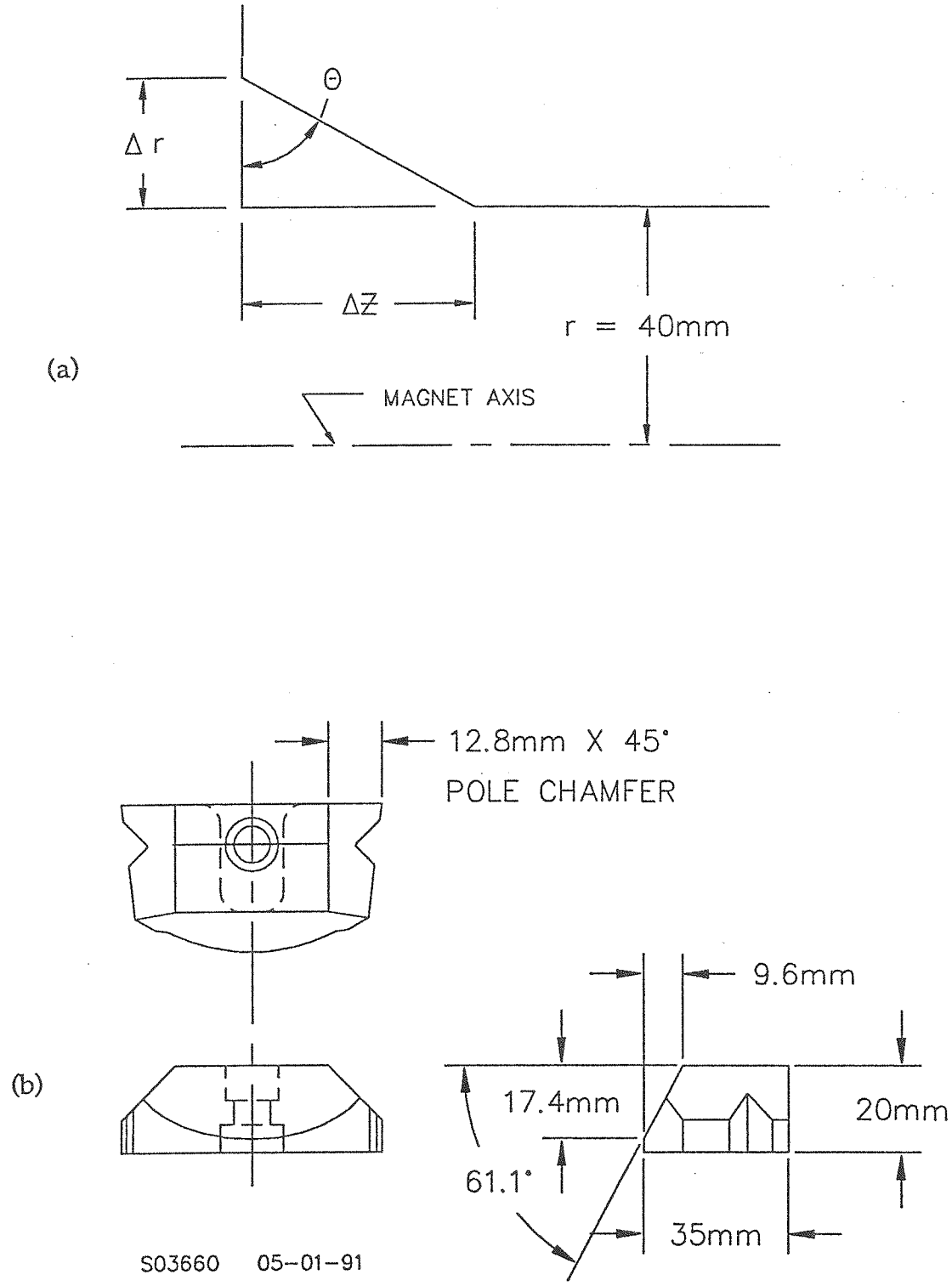

Fig. 7. Pole-end bevel geometry (a) and a removable pole-tip with pole-end bevel, Δr = 9.6 mm, Δz = 17.4 mm, θ = 61.1°, with 12.8 mm - 45° pole chamfer (b).

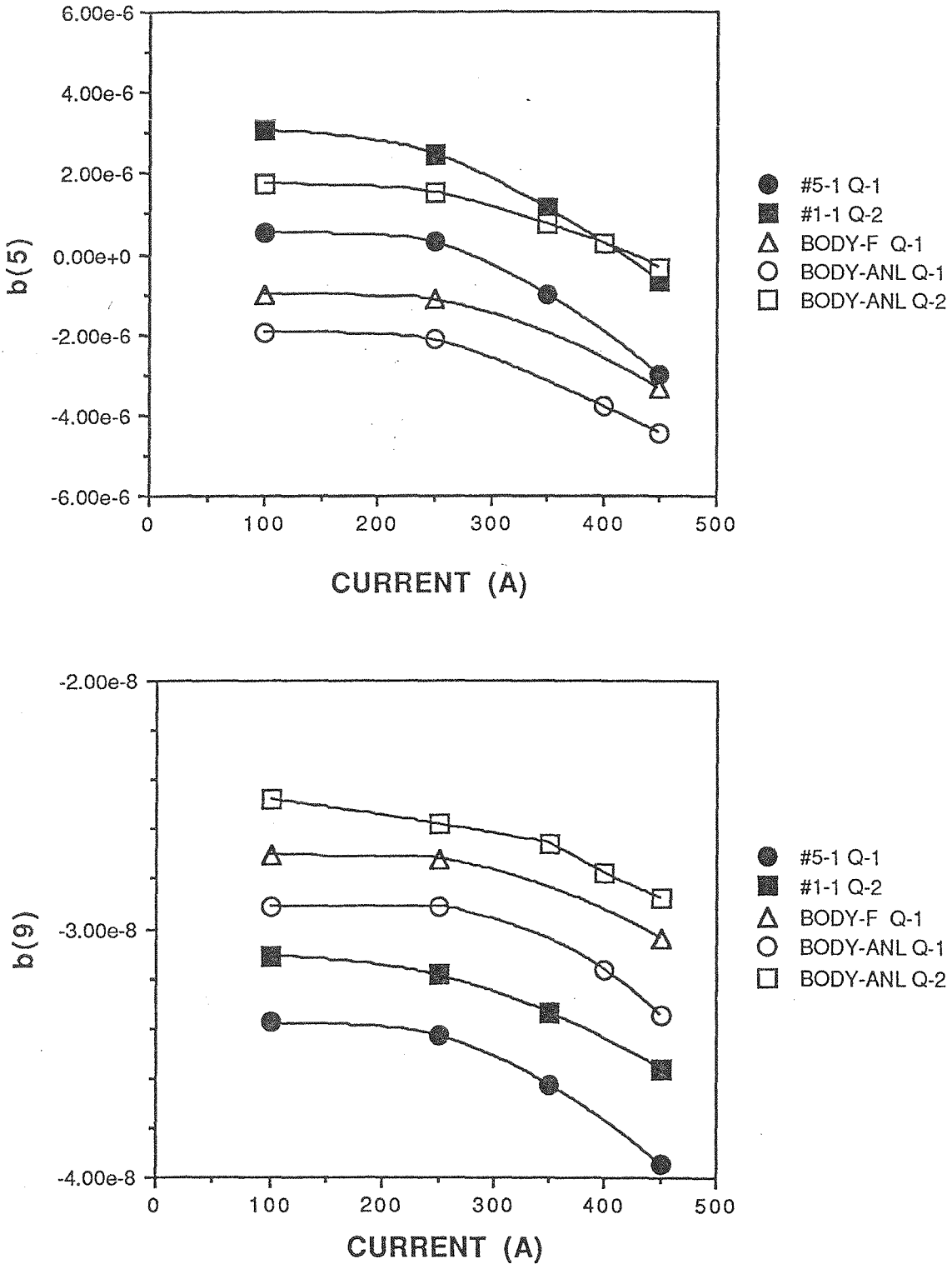

Fig. 8. Duodecapole and 20-pole coefficients of the magnetic length integral measurements (#5-1 Q-1 and #1-1 Q-2) and of the body measurements (BODY-F Q-1, BODY-ANL Q-1 and BODY-ANL Q-2) for the two magnets.

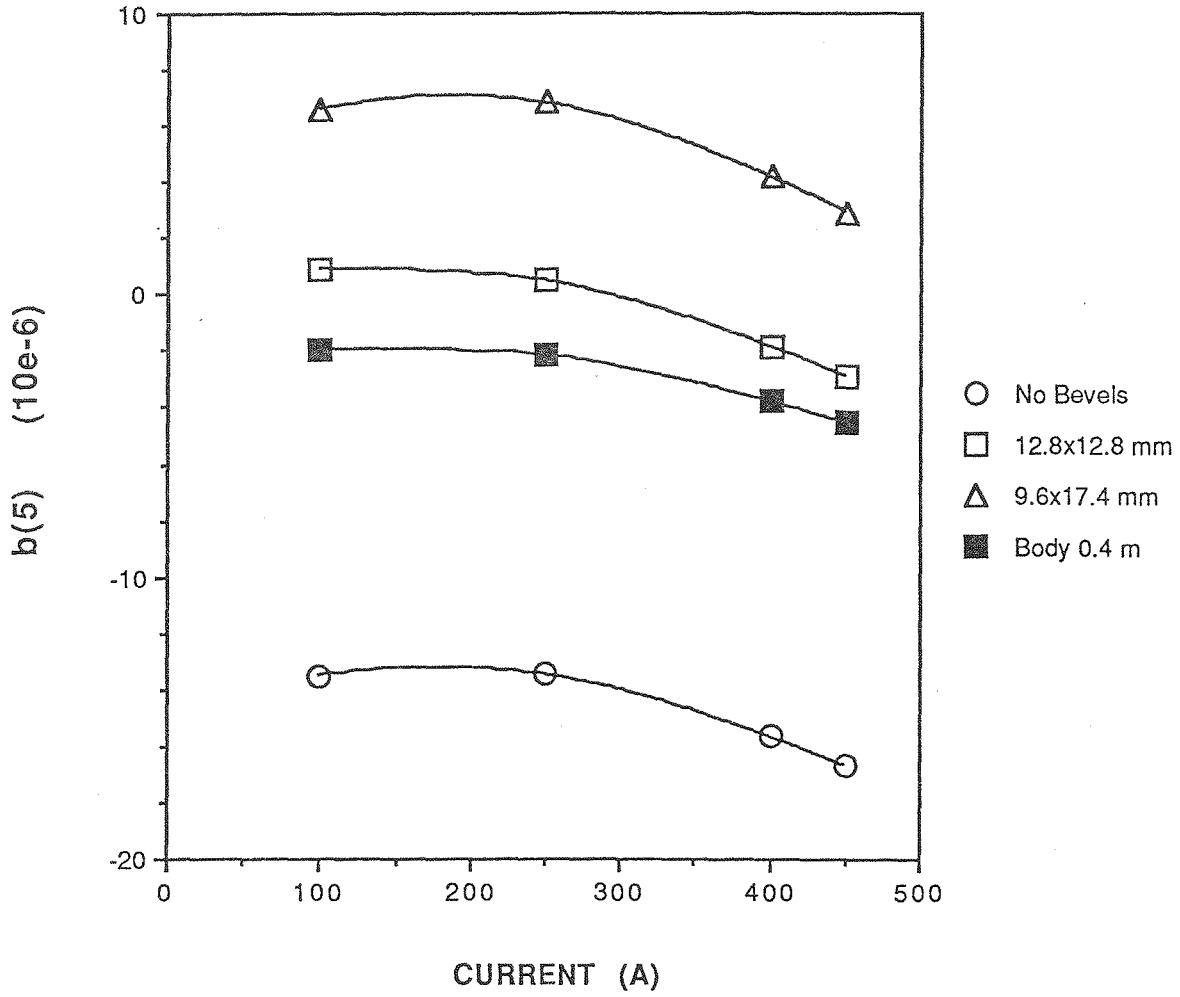

Fig. 9. Dependence of duodecapole coefficient on the pole-end bevel geometries and body values for P-SRQ-1. The body measurent data is for 0.4-m middle section of the magnet. Others are for integral measurements.

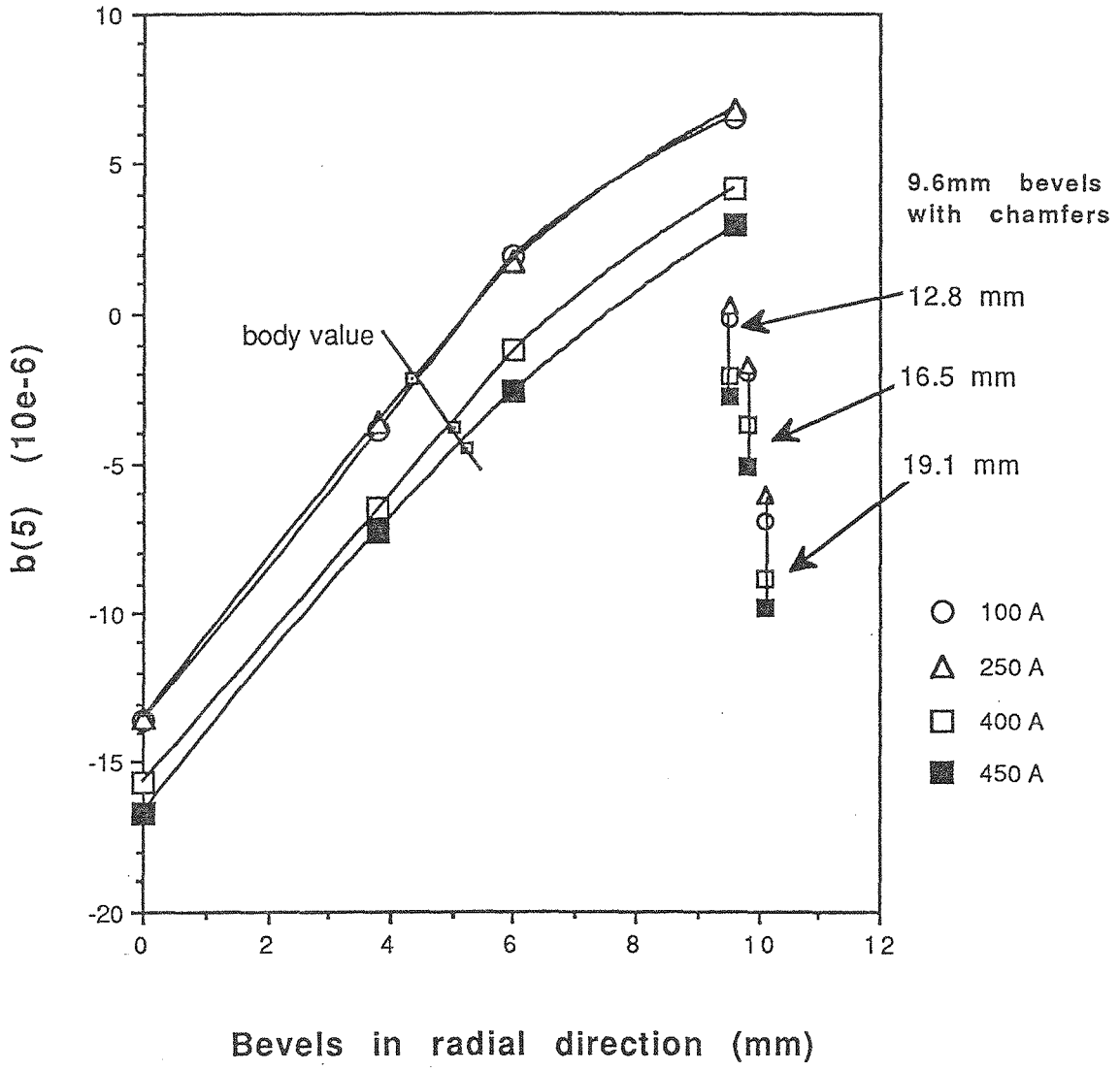

Fig. 10. Dependence of duodecapole coefficient on the pole-end bevels and pole chamfers. Bevel angle, shown in Fig. 7 as θ, is 61.1°. Parameter in the horizontal axis is defined in Fig.7 as Δr. The data for the three pole chamfers are for the bevels with Δr = 9.6 mm, Δz = 17.4 mm.